Korean J. Chem. Eng., 32(3), 494-500 (2015)
DOI: 10.1007/s11814-014-0250-9

pISSN: 0256-1115
eISSN: 1975-7220

Molecular dynamics simulation of carbon molecular sieve preparation for air separation

Elham Yaghoobpour*, Ali Ahmadpour*, Nafiseh Farhadian*,†, and Mojtaba Shariaty-Niassar**

*Department of Chemical Engineering, Faculty of Engineering, Ferdowsi University of Mashhad, Mashhad, Iran
**Department of Chemical Engineering, School of Engineering, University of Tehran, Tehran, Iran
(*Received 6 May 2014 • accepted 26 August 2014*)

Abstract−Carbon deposition process on activated carbon (AC) in order to produce carbon molecular sieve (CMS) was simulated using molecular dynamics simulation. The proposed activated carbon for simulation includes micropores with different characteristic diameters and lengths. Three different temperatures of 773 K, 973 K, and 1,273 K were selected to investigate the optimum deposition temperature. Simulation results show that the carbon deposition process at 973 K creates the best adsorbent structure. While at lower temperature some micropore openings are blocked with carbon atoms, at higher temperature the number of deposited carbons on the micropores does not change significantly. Also, carbon deposition process confirms the pseudo-second-order kinetic model with an endothermic behavior. To evaluate the sieving property of adsorbent products, nitrogen and oxygen adsorption on the initial and final adsorbent products are examined. Results show that there is not any considerable difference between the equilibrium adsorption amounts of nitrogen and oxygen on the initial and final adsorbents especially at low pressure (P<10 atm). Although, adsorption kinetics curves of these gases change significantly after the carbon deposition process in comparison with the initial sample. These observations indicate that the final adsorbent has high selectivity towards oxygen compared with the nitrogen, so it can be called a carbon molecular sieve. All simulated results are in good agreement with experiments.

Keywords: Carbon Molecular Sieve, Molecular Dynamics Simulation, Carbon Deposition, Adsorption Kinetics, Air Separation

INTRODUCTION

Carbon adsorbents are one of the most popular adsorbent types for gas and liquid separation equipment [1-6]. Easy accessibility, low cost and other individual properties of the carbon adsorbents make them crucial materials in separation processes [2,5]. Carbon molecular sieves (CMS) are a special class of the carbon materials, widely used in gas separation system such as methane from carbon dioxide [3,4], ethane from ethylene [7,8], propane from propylene [9,10], and hydrogen from gas mixture [11,12]. In particular, carbon molecular sieves are used for the air separation to its components, nitrogen (N_2) and oxygen (O_2), on a wide scale [3,13-15].

Many different carbon-based materials, like agricultural residues and biomasses, are applied as precursors in the CMS production step [2,4,6]. Pore size control has been examined by a variety of heat treatment methods, such as carbonization, physiochemical activation, and chemical vapor deposition (CVD), to achieve a structure with efficient sieving properties [4,14,16-18]. It is indicated that controlling the carbon deposition process on the initial pores has a major effect on the resulted material's structure. However, because of the practical and limited conditions of the experiments, some parameters which are impossible to measure can be traced and investigated by the computational means. In addition, some simulation methods help us to find the optimum experimental conditions. Therefore, complicated and costly serial experiments can be ignored. In this regard, the theoretical methods have been developed to carry out studies on the carbon adsorbents. In recent decades, molecular simulation methods such as Monte Carlo (MC) and molecular dynamics (MD) simulation have been successfully employed to simulate the adsorption process [19-25]. Moreover, the formation process of carbon adsorbent can be simulated; for instance, the quench MD simulation method has been applied to simulate CMS formation process using different precursors [26]. Based on this method, a realistic model for amorphous carbon has been developed [27,28]. Furthermore, the CVD process on the active carbon to produce a CMS structure has been modeled using the stochastic method, allowing one to investigate the amount of deposited carbon versus time [29]. Despite these studies, there is a lack of molecular information in this area. Developing a suitable atomistic model that realistically describes the carbon deposition process on the pores in the molecular level is necessary. Furthermore, the capability of the resulted CMS structures for target separation can be considered as a crucial item for detailed investigations.

We used molecular dynamics (MD) simulation to investigate carbon deposition on activated carbons and examine the performance of the resulting material to segregate air into its components on a molecular scale. The objectives of this paper are:

(i) Modification of activated carbon by carbon deposition in the molecular level;

(ii) Analyzing the temperature role on the pore deposition;

†To whom correspondence should be addressed.
E-mail: n.farhadian@um.ac.ir, na.farhadian@gmail.com

(iii) Calculating some thermodynamics parameters like enthalpy, entropy and Gibbs free energy in carbon deposition process; and

(iv) Evaluating the modified product behavior for nitrogen and oxygen separation by determining the isotherm and kinetic curves.

MOLECULAR MODEL AND FORCE FIELD

Molecular dynamics simulations are performed to simulate the formation of carbon molecular sieve by carbon deposition on an activated carbon. Also, N_2 and O_2 adsorption on the initial proposed AC and resulted material are investigated.

1. Molecular Model and Simulation Parameters

Since activated carbon does not have a certain crystallography structure, it is assumed that its structure in the molecular scale is constructed of the graphene layer sheets with various orientations. Hence, the applied structure is composed of four graphene-based slit micropores inside a mesopore with the pore width of about 25 Å.

In the proposed structure, the micropores include two pores with characteristic diameters (the distance between graphene slits) of 7 Å and depths of 13.5 and 27 Å and two other pores with diameter of 5 Å and depths of 13.5 and 27 Å. These dimensions are applied to investigate the effects of pore width and depth on the adsorbent capacity. It is noted that the microporous (characteristic diameters less than 2 nm) or the mesoporous (characteristic diameters 2-50 nm) mainly are responsible for gas separation. In practice, strong adsorption occurs in these pores, specially micropores. Adsorption in macropores (characteristic diameters larger than 50 nm) is similar to what occurs on the adsorbent surface, and they work as conduits for gas transferring to smaller pores in separation processes. Hence, only micro- and mesopores are assumed in the structure. According to the experimental data, the size of the graphene layer is between 20 and 70 Å [30], so the largest linear dimension of graphene layer has been chosen as 65.38 Å. The proposed structure is depicted in Fig. 1. Simulation is conducted in a box with the dimensions of 22.35×55.48×67.39 $Å^3$. The interlayer spacing between graphene layers consisting of pore wall is 3.335 Å according to literature data [31-33]. Simulations are performed at two different parts:

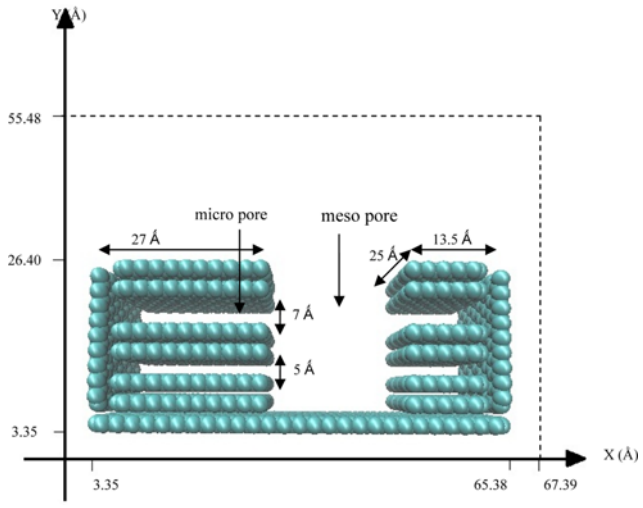

Fig. 1. Proposed AC structure with the box dimensions.

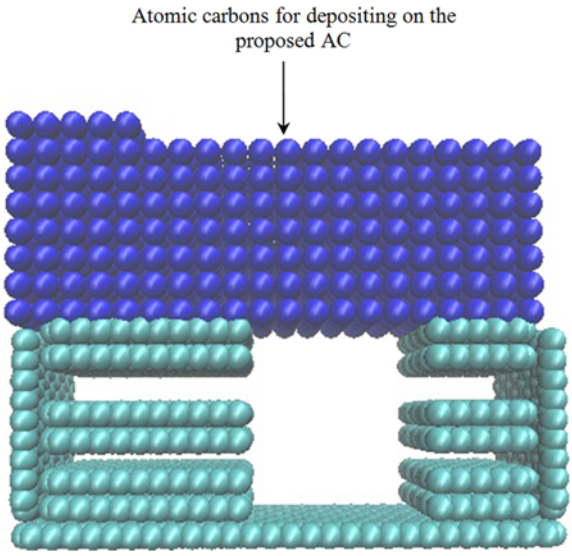

Fig. 2. Simulation structure in carbon deposition part (atoms are shown with VDW model in the graphical software).

i) Carbon deposition on the AC structure. Atomistic carbons are employed for depositing on the proposed AC. It is assumed that the atomistic carbons have resulted from benzene cracking process accorded with ref. [30]. Note that the benzene cracking process to produce carbon atoms for deposition is neglected from MD simulation. According to the experimental data, the density ratio of AC to the atomistic carbons for deposition is 3/1 [30]. Therefore, for 2168 carbon atoms as the graphene sheet in the AC structure, 723 atomistic carbons are devoted for deposition. These atoms are placed on the top of AC pores before the simulation (Fig. 2).

ii) N_2/O_2 adsorption by determining adsorption isotherm and kinetic curves. To achieve this goal, different MD simulations are performed at constant temperature and volume with different numbers of N_2 and O_2 molecules for initial AC and CMS product.

All MD simulations were performed in canonical ensemble (*NVT*). In the first part (carbon deposition on the AC), three simulations investigated the effect of temperature on the carbon deposition process. In all simulations, the volume and number of atoms were constant. Selected temperatures according to the experimental data [30] were 773, 973, and 1,273 K. In all simulations, the volume and number of atoms were constant. In part (ii) (N_2/O_2 adsorption), two different adsorbents, the initial proposed AC structure and resulting adsorbent after carbon deposition, were applied. At this stage and for calculating adsorption isotherms, twelve simulations were performed to create different N_2 and O_2 pressure in the box (six simulations for calculating each N_2 and O_2 isotherms). Different pressures (3 atm<P<22 atm) are created by changing the number of gas molecules while SRK equation of state governs the simulation systems. This procedure has been used in similar MD studies [34,35]. Volume and temperature of the system were constant in all simulations. Temperature was selected as 300 K. The Nose-Hoover [36] thermostat model was applied to maintain the temperature during the simulations. The cut-off distance of 1.2 nm was selected for calculating the non-bonded interactions. Periodic

boundary conditions were applied in all three directions, and the adopted simulation time is 5 ns with the time-step of 2 fs.

All MD simulations were conducted by GROMACS 4.5.5 package [37]. Although GROMACS performs the MD simulation, it can also perform the energy minimization (EM) to make sure the provided structure is properly energy minimized. Thus, before the main MD simulations, the EM stage was performed for 200 ps with a time step of 1 fs. All the graphics in figures are visualized by VMD package [38].

2. Force Field

The interactions between molecules in this study, i.e, O_2, N_2, atomistic carbon, and Graphene sheet atoms, were modeled by GROMOS 96 [39] force field. According to GROMOS96 force field, the interactions between the atoms are divided into non-bonded and bonded. Non-bonded interactions are between any pair of atoms within a given cutoff radius presented by Lennard-Jones (12-6) (LJ) potential and other atoms out of the cut off radius are excluded from calculations. In the current simulation, graphene layer is assumed without partial charge. In addition, N_2 and O_2 are assumed electrically neutral . Thus electrostatic interactions were omitted from the calculations.

The nonbounded interaction will be included:

$$U_{nb}=\sum_{i<j}\left\{4\varepsilon_{ij}\left[\left(\frac{\sigma_{ij}}{r_{ij}}\right)^{12}-\left(\frac{\sigma_{ij}}{r_{ij}}\right)^{6}\right]\right\}, \quad (1)$$

where r_{ij} is the interparticle distance, ε_{ij} is the LJ energy and σ_{ij} is the size parameter. Values of the parameters are σ_{ij}=3.360, 2.625, and 2.975 Å and ε_{ij}=0.406, 1.724, and 0.877 kJ/mol for C, O, and N, respectively [40].

Bonded interactions between atoms connected chemically consist of stretching, covalent bond angle, and the dihedral terms. This potential energy U_b is written as:

$$U_b=U_s+U_\theta+U_\phi, \quad (2)$$

where U_s is bond-stretching and given by

$$U_s=\sum_{bonds\ ij}\frac{1}{2}k_{ij}(r_{ij}-l_0)^2, \quad (3)$$

here r_{ij} is center to center distance of atoms i and j, l_0 equilibrium bond length, and k_{ij} force constant. For C-C in the graphene layers, O-O in O_2 molecules, and N-N in N_2 molecules, the value of parameters are, l_0=1.37, 1.208, and 1.098 Å and $k_{ij}=4.18\times10^5$, 4.18×10^5, and 9.45×10^5 kJ/mol nm^2 for C-C, O-O, and N-N, respectively [40].

Potential of bond angle changes U_θ is given by

$$U_\theta=\sum_{\theta_{ijk}}\frac{1}{2}k_{\theta_{ijk}}(\theta_{ijk}-\theta^0_{ijk})^2, \quad (4)$$

where θ^0_{ijk} is the angle in equilibrium and $k_{\theta_{ijk}}$ force constant. For C-C-C the values of parameters are θ_{ijk}=120° and $k_{\theta_{ijk}}$=418.4 kJ/mol rad^2 [40].

Torsional rotational potential U_ϕ representing potential energy associated with dihedral angle changes, is a periodic function given by:

$$U_\phi=\frac{1}{2}k_\phi[1+\cos(m\phi-\phi_0)], \quad (5)$$

where k_ϕ, m, ϕ_0, is a force constant, the dihedral multiplicity, and the equilibrium value of angle, respectively. In present simulation, the value of k_ϕ is k_ϕ=15.15 kJ/mol for C-C-C-C. The values of parameters m and ϕ_0 are taken to be m=3 and ϕ_0=180° [40].

In this study, the self-diffusion of atomistic carbons and also N_2 and O_2 molecules inside pores was investigated. According to a previous study [41], the frozen and flexible structures of graphitic slit pores have very similar effect when self-diffusivity is investigated. It has been also reported that the structure of the pore walls (frozen or flexible) has little effect on kinetic separation factors of binary mixture in graphitic slit pores; while the temperature of the system and the pore size strongly influence it [42]. Hence, the frozen structure was selected for graphitic layers.

RESULTS AND DISCUSSION

In all simulations, it is necessary to show the system equilibration. To do so, total energy at both carbon deposition and N_2/O_2 adsorption simulations is monitored. Results are shown in Figs. 3(a) and 3(b). As the figures show, systems are fully equilibrated in less than 50 ps, so further analyses can be performed.

1. Carbon Deposition Analysis

1-1. Carbon Deposition

In the first step, it was necessary to remove unadsorbed carbon atoms in the deposition process. To do this, the distance criterion for counting the deposited carbon was chosen based on the radial distribution function (RDF) curve (g(r)). The RDF yields the prob-

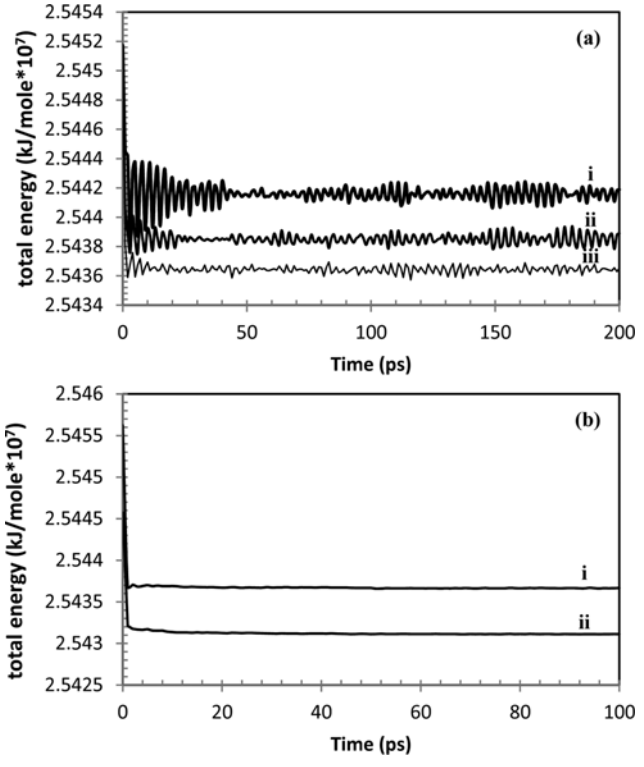

Fig. 3. Total energy curve for (a) carbon deposition process at (i) 1,273 K, (ii) 973 K, and (iii) 773, and (b) total energy curve for (i) O_2 adsorption (ii) N_2 adsorption.

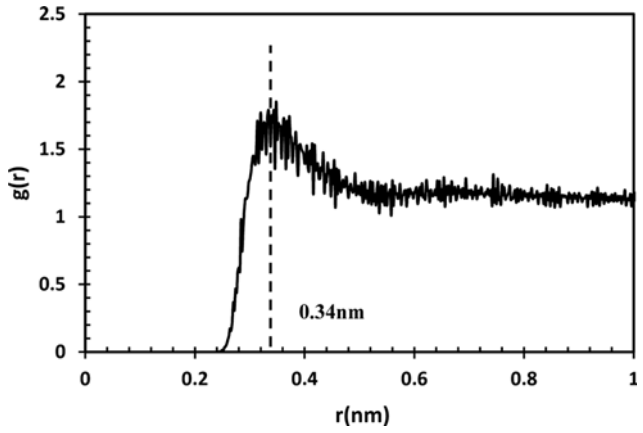

Fig. 4. RDF curve of atomic carbons versus graphitic carbon atoms. This curve is plotted for atomic center of mass.

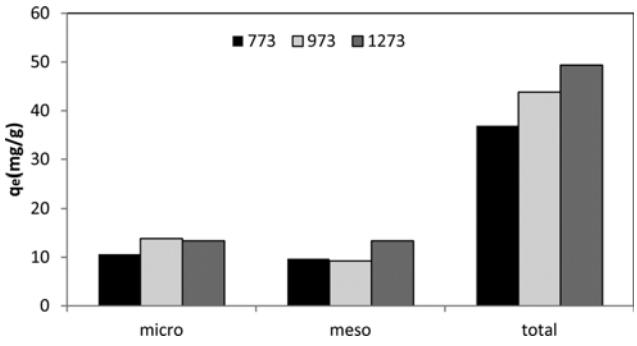

Fig. 6. Amounts of deposited carbon in micropores, mesopores and proposed AC at temperatures of 773 K, 973 K, and 1,273 K.

ability of existence of a particle in a certain distance (r) from other particles. The first peak of the RDF implies minimum distance between deposited carbon and graphitic adsorbent. The RDF for deposited carbon atoms at 773 K versus their distance from graphitic adsorbent is shown in Fig. 4. This figure expresses that the first peak of g(r) occurred in r=0.34 nm. Similar values were obtained at other temperatures. Accordingly, the carbon atoms in 0.34 nm distance of the AC remain in system as the deposited carbon, and the others are removed. This simulation stage is equivalent to what happens in experiment [30]. In other words, removing undeposited carbon from the simulated system based on the RDF curve is similar to nitrogen flow in the experiment for eliminating the unadsorbed carbon atoms on the substrate. Fig. 5 shows schematics of the resulting adsorbents obtained after carbon deposition at different temperatures, and Fig. 6 shows the amount of deposited carbon atoms on the micropore, mesopore and both of them versus adsorbent mass. From Fig. 5, there is not any deposited carbon inside micropore with the characteristic diameter of 5 Å. At lower temperature, these micropores are blocked with the carbon atoms, while at higher temperature there is not any deposited carbon on the mouth of the pores. In contrast, carbons are diffused inside pores with the characteristic diameters of 7 Å, and consequently change size of the pores. Furthermore, multilayer carbon deposition occurred in mesopore, whereas one layer deposition happened in micropores. Also, Fig. 6 shows that by increasing the temperature from 773 K to 1,273 K, the total amount of deposited carbons on the mesopores increased, while this value initially increased for micropores and then decreased at higher temperature. But, totally increasing the temperature increased the total amount of deposited carbons on meso- and micropores, which indicates an endothermic process. Since in N_2/O_2 separation by CMS, micropores play a key role in the separation efficiency, the produced adsorbent from the system in the temperature of 973 K is selected for N_2/O_2 adsorption.

1-2. Kinetic Model of Carbon Deposition

To model the dynamics of the deposition process, kinetics of the process was studied. Two kinetic models, the pseudo-first- and second-order models, were used for the deposition kinetic data to investigate the behavior of this process. In pseudo-first-order model [43], the adsorption kinetics rate is simply determined based on the adsorption capacity using the following equation:

$$\frac{dq_t}{dt} = K_1(q_e - q_t) \tag{6}$$

where q_t and q_e (mg/g) are amount of adsorption at any time t (min) and adsorption capacity in equilibrium corresponding to the monolayer adsorption, respectively. K_1 (min^{-1}) is the rate constant of the pseudo-first-order adsorption.

In the pseudo-second-order model, the adsorption kinetic data is described by:

$$\frac{t}{q_t} = \frac{1}{V_0} + \frac{1}{q_e}t, \tag{7}$$

$$V_0 = K_2 q_e^2 \tag{8}$$

where V_0 (mg/g·min) is the initial rate of adsorption [44].

These two models are examined for the carbon deposition results. Constant values of the kinetic models are calculated from the linear forms of the above-mentioned equations. Results are shown

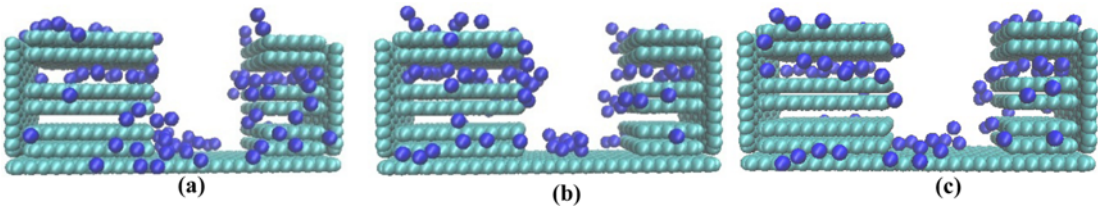

Fig. 5. The resulting structure after carbon deposition process from the front view at (a) 773 K, (b) 973 K, and (c) 1,273 K.

Table 1. Pseudo-first-order and pseudo-second order calculated parameters for carbon deposition process

T (K)	Pseudo-first-order model			Pseudo-second-order model		
	k_1 (1/ns)	q_e (mg/g)	R^2	k_2 (g/mg·ns)	q_e (mg/g)	R^2
773	1.20	2.39	0.421	3.41	38.31	0.991
973	1.10	7.89	0.782	0.43	44.05	0.994
1273	0.10	9.16	0.240	0.25	46.73	0.988

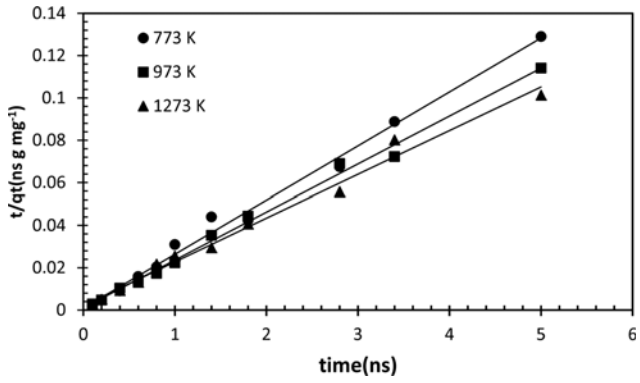

Fig. 7. Pseudo-second-order kinetic model plots for carbon deposition process on the proposed AC at (a) 773 K, (b) 973 K, and (c) 1,273 K.

in Table 1: the pseudo-second-order kinetic model can predict the calculated results carefully (R^2>0.98). Fig. 7 confirms these results.

1-3. Thermodynamic Parameters

The thermodynamic parameters including change in standard Gibbs free energy (ΔG^0), entropy (ΔS^0), and enthalpy (ΔH^0) are obtained from the following equations [45]:

$$K_c = \frac{c_e}{q_e} \tag{9}$$

$$\Delta G^0 = -RT\ln K_c \tag{10}$$

$$\ln K_c = \frac{\Delta S^0}{R} - \frac{\Delta H^0}{RT} \tag{11}$$

here K_c (g/L) is the standard thermodynamic equilibrium constant defined by the ratio of deposited carbon concentration in equilibrium q_e (mg/g), and the equilibrium concentration of carbon in bulk C_e (mg/L). The values of ΔH^0 and ΔS^0 are extracted from the slope and intercept of Eq. (11), respectively. Results are presented in Table 2 (figure is not shown). Positive value for ΔH^0 confirms an endothermic process, which is in agreement with our previous results (see section 3.1.1). The positive value of ΔS^0 elaborates increasing of randomness at the solid/gas interface. In addition, the negative values of ΔG^0 at different temperatures describe the spontaneous nature of the process.

Table 2. Thermodynamic parameters of carbon deposition process on AC

ΔS^0 (J/mol·K)	ΔH^0 (J/mol)	ΔG^0 (J/mol)		
68.73	4768	773 K	973 K	1273 K
		−57942	−71543	−92343

2. N_2/O_2 Adsorption Analysis

2-1. Adsorption Isotherm

In this stage, adsorption isotherms are calculated for N_2 and O_2 gas molecules, separately on the initial proposed AC and resulting adsorbents. The produced structure after carbon deposition at 973 K is applied for this goal. Fig. 8 shows the isotherm curves. From this figure, it can be found that at low pressure (p<10 atm), the adsorption amounts of N_2/O_2 gases on the two types adsorbents are equal. At high pressure, the amount of adsorbed O_2 on the resulting adsorbent increases in comparison to the initial proposed AC, while the amount of adsorbed N_2 on the resulted adsorbent decreases. However, these changes are not significant. Considering the kinetic diameters of O_2 and N_2 which are too close (d_{O_2}=3.46 Å and d_{N_2}= 3.64 Å), their equilibrium concentrations on the adsorbent are approximately equal. This supports the results reported in [30]. These changes in N_2/O_2 adsorption amounts are not too high to create reasonable separation efficiency for these two gases.

Additionally, the two isotherm models, Langmuir and Freundlich, have been applied to model the isotherm data.

The Langmuir equation and its linear form are given as [43]:

$$q_e = \frac{bQ_0P}{bP+1} \tag{12}$$

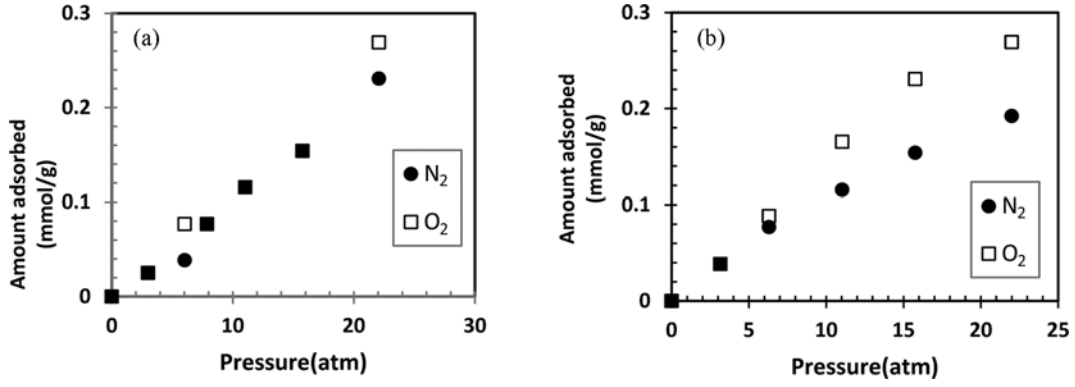

Fig. 8. N_2 and O_2 isotherm curves on the (a) proposed AC, and (b) resulting adsorbent.

Table 3. Langmuir and Freundlich isotherm parameters for N_2 and O_2 adsorption on the resulted adsorbent

	Freundlich isotherm			Langmuir isotherm	
	K_F	n	R^2	Q_0	R^2
O_2	0.0116	0.95	0.990	0.019	0.996
N_2	0.0157	1.21	0.993	0.021	0.999

$$\frac{1}{q_e}=\frac{1}{Q_0}+\frac{1}{bQ_0P} \tag{13}$$

where q_e, Q_0, and b are adsorption capacity in equilibrium, maximum capacity of adsorption corresponding to complete monolayer coverage, and adsorption affinity, respectively.

The Freundlich model is an empirical model with the following equation [46]:

$$q_e=K_F P_e^{1/n} \tag{14}$$

Its linear form is:

$$\log q_e=\log K_F+\frac{1}{n}\log P_e \tag{15}$$

where q_e is adsorbate concentration at equilibrium, P_e is pressure, and K_F is Freundlich constant. Table 3 shows calculated parameters of both models for N_2 and O_2 adsorption on the resulted adsorbent. As illustrated, the adsorption processes strongly follow the Langmuir isotherm model (R^2>0.996). This adequate conformation demonstrates the homogeneous nature of the adsorption surface. Fig. 9 shows the linear fitting of N_2/O_2 isotherm with Langmuir equation.

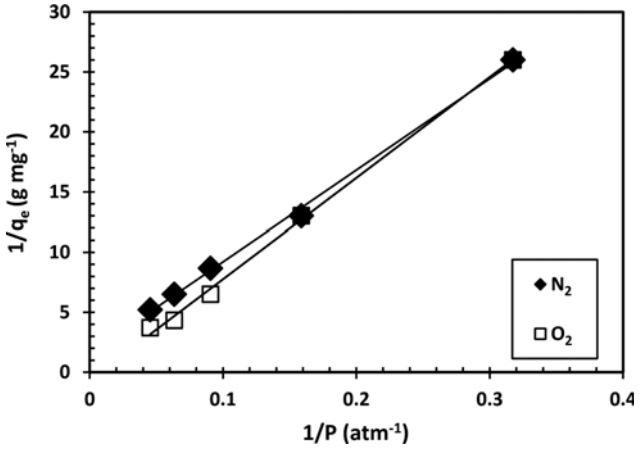

Fig. 9. Langmuir isotherm in the linear form for N_2/O_2 adsorption on the resulting adsorbent.

2-2. Adsorption Kinetics

Although the main criterion in the separation processes is the difference in equilibrium concentration of the adsorbates, this is not a practical criterion for the N_2/O_2 separation processes. Thus, the performance of the CMS adsorbent for the N_2/O_2 separation should be determined by the adsorption kinetics [47]. So, adsorption kinetics curves of N_2/O_2 on the proposed AC and resulting adsorbent at the pressure of 14 atm are investigated (Figs. 10 and

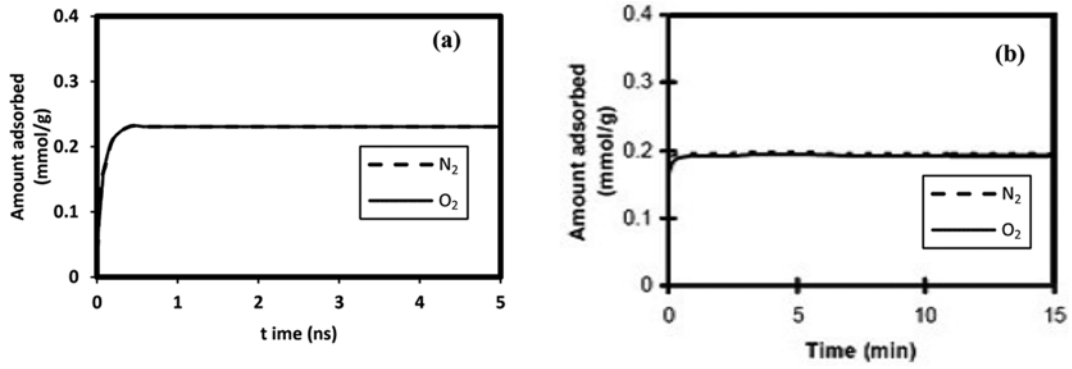

Fig. 10. Adsorption kinetic curves of N_2/O_2 gases on the (a) proposed AC, and (b) experimental AC sample [30].

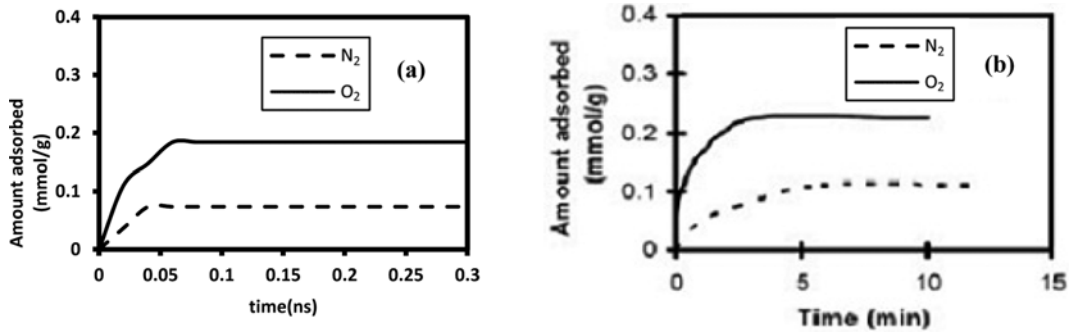

Fig. 11. Adsorption kinetic curves of N_2/O_2 gases on the resulted adsorbent in (a) simulation, and (b) experiment [30].

11). From Fig. 10(a), the amounts of adsorbed N_2 and O_2 on the proposed AC at all the times are equal to each other. In other words, no separation has occurred by this simulated adsorbent. Interestingly, adsorption kinetics curves on the resulting adsorbent for both N_2/O_2 gases versus time have been significantly changed, which may create a good separation efficiency (Fig. 11(a)). O_2 with smaller kinetic diameter adsorbs faster than N_2 on the produced adsorbent. These observations are exactly matching the experimental results (Fig. 10(b) and 11(b)) [30]. Finally, it can be concluded that the resulting adsorbent has a molecular sieve behavior.

CONCLUSIONS

The carbon deposition process on a proposed activated carbon structure to produce a carbon molecular sieve adsorbent has been simulated using molecular dynamics simulation method. The purpose of composing a carbon molecular sieve with narrow pore size distribution in the target molecular range is utilization for air separation. Thus, the capability of resulting adsorbent to segregate air to its component is investigated as the second goal of this study. Calculated results from carbon deposition process predict that the best temperature for carbon deposition is around 973 K. At this temperature, micropores of the adsorbent, which are mainly responsible for gas separation, change to the narrowest sizes without blocking the pores. Applying this resulting material for N_2/O_2 separation creates significant differences between N_2/O_2 adsorption kinetics curves, which confirms the sieving mechanism of the resulting adsorbent, whereas the equilibrium isotherms are essentially the same for both N_2 and O_2.

REFERENCES

1. C. M. Castilla, *Carbon*, **42**, 83 (2004).
2. A. Demirbas, *J. Hazard. Mater.*, **167**, 1 (2009).
3. J. M. Valente Nabais, P. J. M. Carrott, M. M. L. Ribeiro Carrott, A. M. Padre-Eterno, J. A. Menéndez, A. Dominguez and A. L. Ortiz, *Carbon*, **44**, 1158 (2006).
4. D. Adinata, W. M. A. W. Daud and M. K. Aroua, *Fuel Process Technol.*, **88**, 599 (2007).
5. L. P. Wang, Z. C. Huang and M. Y. Zhang, *T. Nonferr. Metal. Soc.*, **23**, 530 (2013).
6. B. C. Kim, Y. H. Kim and T. Yamamoto, *Korean J. Chem. Eng.*, **25**, 1140 (2008).
7. M. Rungta, C. Zhang, W. J. Koros and L. Xu, *AIChE J.*, **59**, 3475 (2013).
8. M. Rungta, L. Xu and W. J. Koros, *Carbon*, **50**, 1488 (2012).
9. H. Jarvelin and J. R. Fair, *Ind. Eng. Chem. Res.*, **32**, 2201 (1993).
10. C. A. Grande, V. M. T. M. Silva, C. Gigola and A. E. Rodrigues, *Carbon*, **41**, 2533 (2003).
11. H. H. Tseng and A. K. Itta, *J. Membr. Sci.*, **389**, 223 (2012).
12. A. K. Itta and H. H. Tseng, *Int. J. Hydrog. Energy*, **36**, 8645 (2011).
13. A. R. Mohamed, M. Mohammadi and G. N. Darzi, *Renew. Sust. Energy Rev.*, **14**, 1591 (2010).
14. R. F. P. M. Moreira, H. J. José and A. E. Rodrigues, *Carbon*, **39**, 2269 (2001).
15. C. R. Reid, I. P. O'koye and K. M. Thomas, *Langmuir*, **14**, 2415 (1998).
16. M. Mohammadi, G. D. Najafpour and A. R. Mohamed, *Chem. Ind. Chem. Eng. Q*, **17**, 525 (2011).
17. I. Prasetyo and D. D. Do, *Carbon*, **37**, 1909 (1999).
18. M. Kiyono, P. J. Williams and W. J. Koros, *J. Membr. Sci.*, **359**, 2 (2010).
19. D. D. Do and H. D. Do, *Colloids Surf., A*, **252**, 7 (2005).
20. L. F. Herrera, D. D. Do and G. R. Birkett, *J. Colloid Interface Sci.*, **320**, 415 (2008).
21. T. Okayama, J. Yoneya and T. Nitta, *Fluid Phase Equilib.*, **104**, 305 (1995).
22. M. Georgakis, G. Stavropoulos and G. P. Sakellaropoulos, *Micropor. Mesopor. Mater.*, **191**, 67 (2014).
23. Y. Liu and J. Wilcox, *Int. J. Coal Geol*, **104**, 83 (2012).
24. C. Fan, D. D. Do, D. Nicholson, J. Jagiello, J. Kenvin and M. Puzan, *Carbon*, **52**, 158 (2013).
25. A. T. Nasrabadi and M. Foroutan, *Comp. Mater. Sci.*, **61**, 134 (2012).
26. Y. Shi, *J. Chem. Phys.*, **128** (2008).
27. J. C. Palmer, A. Llobet, S.-H. Yeon, J. E. Fischer, Y. Shi, Y. Gogotsi and K. E. Gubbins, *Carbon*, **48**, 1116 (2010).
28. J. C. Palmer, J. K. Brennan, M. M. Hurley, A. Balboa and K. E. Gubbins, *Carbon*, **47**, 2904 (2009).
29. L. T. Fan, A. Argoti, W. P. Walawender and S. T. Chou, *Ind. Eng. Chem. Res.*, **44**, 2343 (2005).
30. A. Ahmadpour, M. Mahdyarfar, A. Rashidi and M. Abedinzadegan Abdi, *Eng. Fac. J-FUM*, **18**, (2007).
31. J. M. D. MacElroy and M. J. Boyle, *Chem. Eng. J.*, **74**, 85 (1999).
32. W. Zhiqiang, L. Zhiping, W. Wenchuan, F. Yiqun and X. Nanping, *Chinese J. Chem. Eng.*, **16**, 709 (2008).
33. P. A. Gauden, A. P. Terzyk, S. furmaniak, J. Wloch, P. Kowalczyk and W. Zielinski, *J. Phys. Condens Matter*, **26**, 1 (2014).
34. S. Vela and F. H. Larrañaga, *Carbon*, **49**, 4544 (2011).
35. M. Foroutann and A. T. Nasrabadi, *Physica E*, **43**, 261 (2010).
36. P. H. Hunenberger, *Adv. Polym. Sci.*, **173**, 105 (2005).
37. B. Hess, C. Kutzner, D. van der Spoel and E. Lindahl, *J. Chem. Theory Comput.*, **4**, 435 (2008).
38. W. Humphrey, A. Dalke and K. Schulten, *J. Mol. Graphics*, **14**, 33 (1996).
39. W. R. P. Scott, P. H. Huenenberger, I. G. Tironi, A. E. Mark, S. R. Billeter, J. Fennen, A. E. Torda, T. Huber, P. Krueger and W. F. van Gunsteren, *J. Phys. Chem. A*, **103**, 3596 (1999).
40. W. F. van Gunsteren and H. J. C. Berendsen, *Angew. Chem. Int. Ed. Engl.*, **29**, 992 (1990).
41. Q. Cai, M. J. Biggs and N. A. Seaton, *Phys. Chem. Chem. Phys.*, **10**, 2519 (2008).
42. L. Xu, G. Sedigh, M. Sahimi and T. T. Tsotsis, *Phys. Rev. Lett.*, **80**, 3511 (1998).
43. S. Lagergren, *Kung Seven Veten Hand*, **24**, 1 (1898).
44. Y. S. Ho and G. McKay, *Process. Biochem.*, **34**, 451 (1999).
45. R. Rahchamani, H. Zavvar Mousavi and M. Behzad, *Desalination*, **267**, 267 (2011).
46. H. M. F. Freundlich, *J. Phys. Chem.*, **57**, 385 (1906).
47. R. T. Yang, *Adsorbents fundamentals and application*, Wiley, New Jersey (2003).